Supporting Information: Surface Reconstruction Tunes Band Edges and Lattice-Oxygen Reactivity on $BiVO_4$(010) Photoanodes

Yonghyuk Lee,[†] Changkyu Cho,[‡] Ki-Tae Lee,[*,‡,¶,§,‖] and Taehun Lee[*,‡,¶,‖]

[†]*Department of Chemical and Biochemical Engineering, Dongguk University, Seoul 04620, Republic of Korea*

[‡]*Division of Advanced Materials Engineering, Jeonbuk National University, Jeonju 54896, Republic of Korea*

[¶]*Department of Energy Storage/Conversion Engineering of Graduate School (BK21 FOUR), Jeonbuk National University, Jeonbuk 54896, Republic of Korea*

[§]*Department of JBNU-KIST Industry-Academia Convergence Research, Jeonbuk National University, Jeonbuk 54896, Republic of Korea*

[‖]*Hydrogen and Fuel Cell Research Center, Jeonbuk National University, Jeonbuk, 54896, Republic of Korea*

E-mail: ktlee71@jbnu.ac.kr; taehun.lee@jbnu.ac.kr

Methods

Computational Details

Hybrid functional calculations were performed with the dielectric-dependent PBE0 functional, fixing the exact-exchange fraction at $\alpha = 1/\epsilon_\infty = 0.22$, following previous benchmarks on $BiVO_4$ showing that this value reproduces quasiparticle-level band gaps and defect energetics.[1–3] For efficient hybrid calculations of the aqueous $BiVO_4$ interfaces, we employed the PBE0–TC–LRC scheme[4] together with the auxiliary density–matrix method (ADMM)[5] in CP2K.[6] Core–valence interactions were described by Goedecker–Teter–Hutter (GTH) pseudopotentials,[7] and molecularly optimized (MOLOPT) double-ζ polarization basis sets were used for Bi, V, and O, with a triple-ζ set for H.[8] A plane-wave density cutoff of 600 Ry was applied, and all supercells were sampled at the Γ-point, consistent with established hybrid functional calculation setups for aqueous $BiVO_4$ interface in earlier studies.[1,9–11]

For simplicity, we modeled the tetragonal phase of $BiVO_4$ (space group $I4_1/a$, $a = 5.172$ Å, $c = 11.771$ Å); its (001) facet is approximately equivalent to the monoclinic (010) surface and captures the bulk band structure and polaron states of the monoclinic phase.[12] The computed band gap (2.72 eV) matches well with reported experimental values (2.5–2.6 eV).[9,13] This tetragonal model has been widely employed in prior theoretical studies because its low-index surfaces and electronic structure closely resemble those of the monoclinic phase, making it a reliable computational proxy for surface and defect modeling.[3,11,14,15] Nevertheless, we acknowledge that the lower symmetry and more distorted VO_4 units in the monoclinic structure could slightly modify the thermodynamic ordering of surface reconstructions.

Six electrochemically stable terminations were examined: **t**-BiO_2 and **t**-BiO_3 (Bi-rich); **t**-$BiVO_4$ and **t**-$BiVO_6$ (stoichiometric/O-rich); and **t**-VO_2 and **t**-VO_4 (V-rich). These surfaces are denoted **t**-$Bi_xV_yO_z$, reflecting the relative ratios of atoms in the outermost layers. Each aqueous $BiVO_4$ interfacial model employed a symmetric $p(2 \times 2)$ slab containing at least ten

$BiVO_4$ trilayers; a ∼15 Å water layer (56 H_2O, matching bulk water density) was added to form the aqueous interface. The initial water configuration was taken from the equilibrated $BiVO_4$(010)/water interface of Ref. 1.

Born–Oppenheimer *ab initio* molecular-dynamics (*ai*MD) simulations were run in the canonical (NVT) ensemble at 350 K (a commonly used choice to avoid over-structured water and to ensure diffusive dynamics at hybrid-DFT accuracy[16,17]) using a Nosé-Hoover chain thermostat, a 0.5 fs timestep, and the D3 dispersion correction.[18] Production trajectories of 7.5 ps were generated for each termination, with electrostatic potentials saved every 50 fs for band-edge analysis. For the equilibrated trajectories, we introduced a single oxygen vacancy (V_O) in the $BiVO_4$ bulk-like region of the aqueous slab, thereby adding two unpaired excess electrons, and followed the equilibration of these excess electronic states for ∼3.0 ps.

SHE/Vacuum-referenced band alignment

We determine the band edges of bulk $BiVO_4$ in water using a hybrid–DFT/electrostatic line-up scheme, following Refs. 11,19. First, the conduction- and valence-band edges are obtained from *ab initio* MD of bulk $BiVO_4$ (supercell $2 \times 2 \times 2$) run for > 10 ps with a 0.5 fs timestep; Kohn–Sham eigenvalues (along with the electrostatic potential needed for the subsequent line-up) are sampled every 50 fs over the last 5 ps to yield time-averaged CBM and VBM at 300 K.

These raw, finite-T band edges are then corrected to account for the spin orbit coupling (SOC), excitonic effects (EE), and nuclear quantum effects (NQE), using shifts from Refs. 11,19 (ΔVBM= +0.50 eV and ΔCBM= −0.43 eV). We write

$$\begin{aligned} \varepsilon_{\mathrm{CBM}}(T) &= \varepsilon^{\mathrm{AIMD}}_{\mathrm{CBM}}(T) + \Delta\varepsilon^{\mathrm{SOC}}_{\mathrm{CBM}} + \Delta\varepsilon^{\mathrm{NQE}}_{\mathrm{CBM}} + \Delta\varepsilon^{EE}_{\mathrm{CBM}}, \\ \varepsilon_{\mathrm{VBM}}(T) &= \varepsilon^{\mathrm{AIMD}}_{\mathrm{VBM}}(T) + \Delta\varepsilon^{\mathrm{SOC}}_{\mathrm{VBM}} + \Delta\varepsilon^{\mathrm{NQE}}_{\mathrm{VBM}} + \Delta\varepsilon^{EE}_{\mathrm{VBM}}. \end{aligned} \tag{S1}$$

The room-temperature fundamental gap then follows as

$$E_g(T) = \varepsilon_{\mathrm{CBM}}(T) - \varepsilon_{\mathrm{VBM}}(T). \tag{S2}$$

The corrected bulk edges are subsequently placed on an absolute scale at the $BiVO_4(010)$/water interface via plane-averaged electrostatic line-up, as in Refs. 11,19.

The bulk band edges depending on the $BiVO_4(010)$/water interface are aligned to the vacuum level and to a computational standard hydrogen electrode (SHE) potential, μ_{SHE}. Following the plane-averaged electrostatic line-up scheme,[20,21] the bulk $BiVO_4$ and water references are obtained by comparing plateau values of the electrostatic potential in bulk-like $BiVO_4$ and water regions in the interface models. Specifically, the potential offsets for $BiVO_4$ and liquid water are defined as

$$\begin{aligned} \Delta V_{\mathrm{BiVO_4}} &= V_{\mathrm{BiVO_4}}(\mathrm{bulk}) - V_{\mathrm{BiVO_4}}(\mathrm{interface}), \\ \Delta V_{\mathrm{water}} &= V_{\mathrm{water}}(\mathrm{bulk}) - V_{\mathrm{water}}(\mathrm{interface})\,, \end{aligned} \tag{S3}$$

where $V_{\mathrm{BiVO_4}}(\mathrm{bulk})$ and $V_{\mathrm{water}}(\mathrm{bulk})$ denote the plateau values from separate bulk calculations and $V_{\mathrm{BiVO_4}}(\mathrm{interface})$ and $V_{\mathrm{water}}(\mathrm{interface})$ are the corresponding plateau values extracted from each bulk-like region of the interface supercells. All potentials are plane-averaged along the surface normal and time-averaged over the last 5 ps of the 10 ps PBE0–*ai*MD bulk $BiVO_4$ trajectory; for interfaces, averages are taken over the last 2.5 ps of the 7.5 ps PBE0–*ai*MD runs.

For surface-derived electronic levels, we do not re-reference to a separate $V_{\mathrm{BiVO_4}}(\mathrm{bulk})$. Instead, the surface-projected Kohn–Sham levels (VBM/CBM or defect states) from the aqueous interface are placed on an absolute scale using only $\Delta V_{\mathrm{water}}$ offsets, enabling a consistent vacuum/SHE comparison with bulk band offsets. The surface-projected VBM/CBM were corrected analogously to the bulk edges, i.e., including SOC, nuclear-quantum, and excitonic effect.

Vacuum-referenced edges are obtained via the interfacial electrostatic line-up (the $\Delta V_{\mathrm{BiVO_4}}$ and $\Delta V_{\mathrm{water}}$ offsets) and by adding the inner potential of bulk water relative to vacuum, $\phi_{\mathrm{water}} \approx 3.7$ eV (Refs. 22,23), yielding $\varepsilon^{\mathrm{vac}}_{\mathrm{VBM}}$ and $\varepsilon^{\mathrm{vac}}_{\mathrm{CBM}}$ for both bulk and surface-projected states.

For referencing to SHE, we employ a neutral interface at the point of zero charge, $\mathrm{pH_{PZC}}$, as in Ref. 20. The VBM at $\mathrm{pH_{PZC}}$ is

$$\varepsilon^{\mathrm{SHE}}_{\mathrm{VBM}}(\mathrm{PZC}) = \varepsilon_{\mathrm{VBM}}(T) - \mu_{\mathrm{SHE}} - \Delta V_{\mathrm{BiVO_4}} + \Delta V_{\mathrm{water}}\,, \tag{S4}$$

and $\varepsilon^{\mathrm{SHE}}_{\mathrm{CBM}}(\mathrm{PZC}) = \varepsilon^{\mathrm{SHE}}_{\mathrm{VBM}}(\mathrm{PZC}) + E_g(T)$. Here $\mu_{\mathrm{SHE}} = -4.44$ eV relative to vacuum at 298 K, and $\mathrm{pH_{PZC}}$ is defined as the pH where the surface has no net charge (Ref. 19). Assuming Nernstian behavior (Ref. 24), band edges at a general pH are obtained via

$$\varepsilon^{\mathrm{SHE}}_{n}(\mathrm{pH}) = \varepsilon^{\mathrm{SHE}}_{n}(\mathrm{PZC}) - 0.059\ \mathrm{eV}\left(\mathrm{pH} - \mathrm{pH_{PZC}}\right), \tag{S5}$$

for $n \in \{\mathrm{VBM}, \mathrm{CBM}\}$.

Figures and Tables

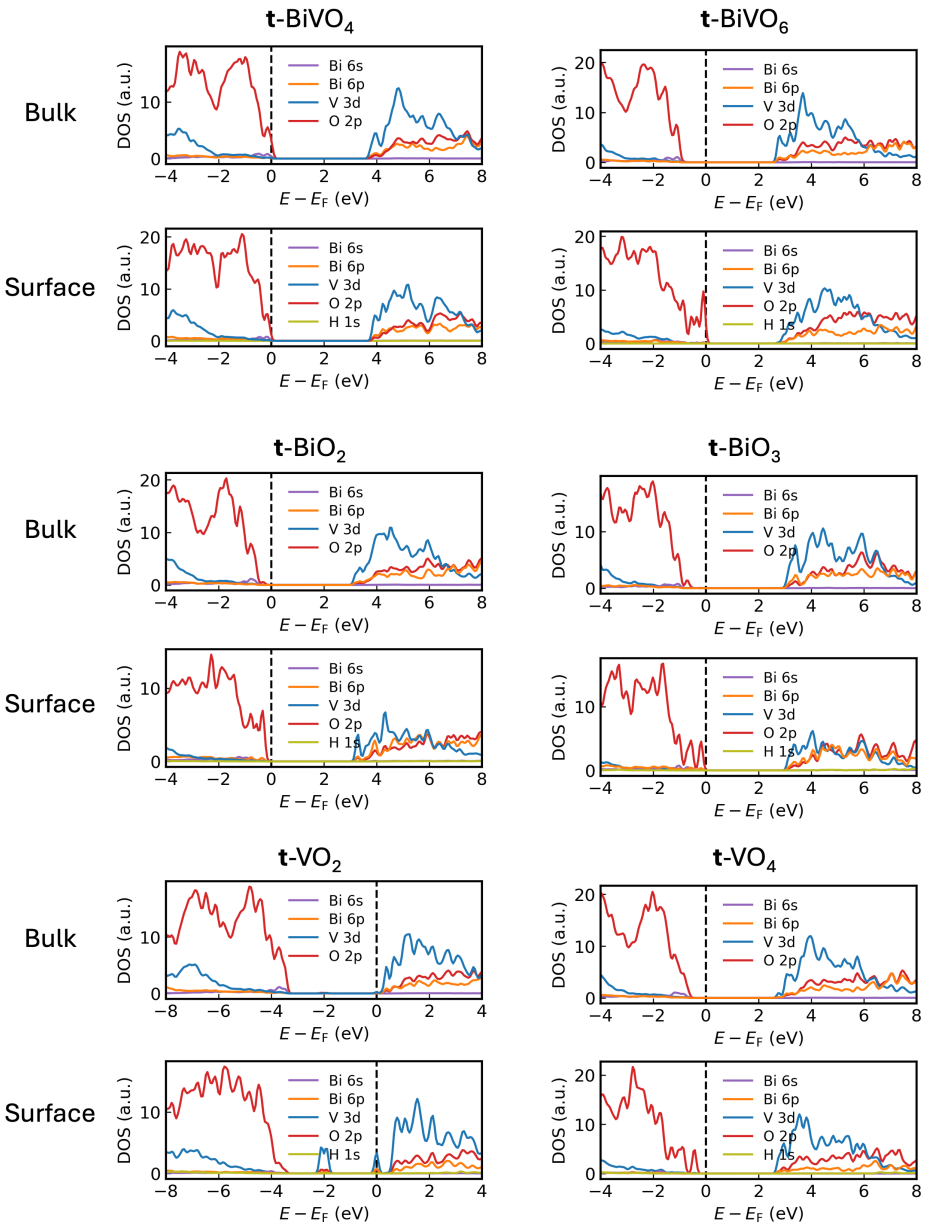

Figure S1: PBE0-computed atom- and orbital-projected density of states at 3 ps for six reconstructed $BiVO_4$(010)/water interfaces. For each termination (**t-**$BiVO_4$, **t-**$BiVO_6$, **t-**BiO_2, **t-**BiO_3, **t-**VO_2, **t-**VO_4), the bulk-like region (top) and the outermost surface layer (bottom) are shown. The surface region is defined as the top two to three cationic layers to capture altered cation–oxygen bonding relative to the stoichiometric surface. Energies are referenced to E_F (vertical dashed line).

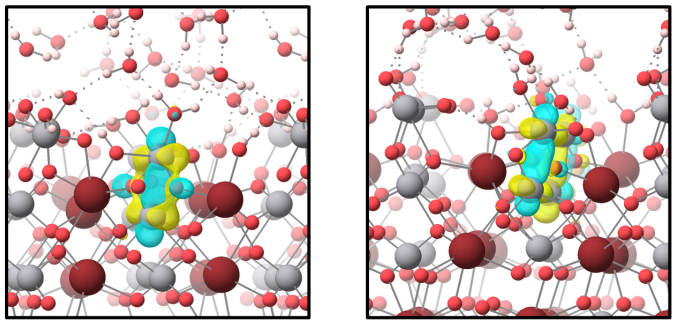

Figure S2: Defect–state charge-density isosurfaces for the aqueous V-rich, oxygen-deficient **t-**VO_2 termination. In this supercell, the V-rich surface stoichiometry yields eight excess electrons (relative to stoichiometric $BiVO_4$) due to oxygen deficiency in the outermost eight V atoms; these localize on surface/subsurface V centers as V^{4+} small polarons, producing V 3*d*–derived mid-gap states in the PDOS (Figure S1). Two representative deep defect (spin-paired) Kohn–Sham states are visualized in the charge-density plots. Bi, V, and O atoms are shown as purple, gray, and red spheres, respectively.

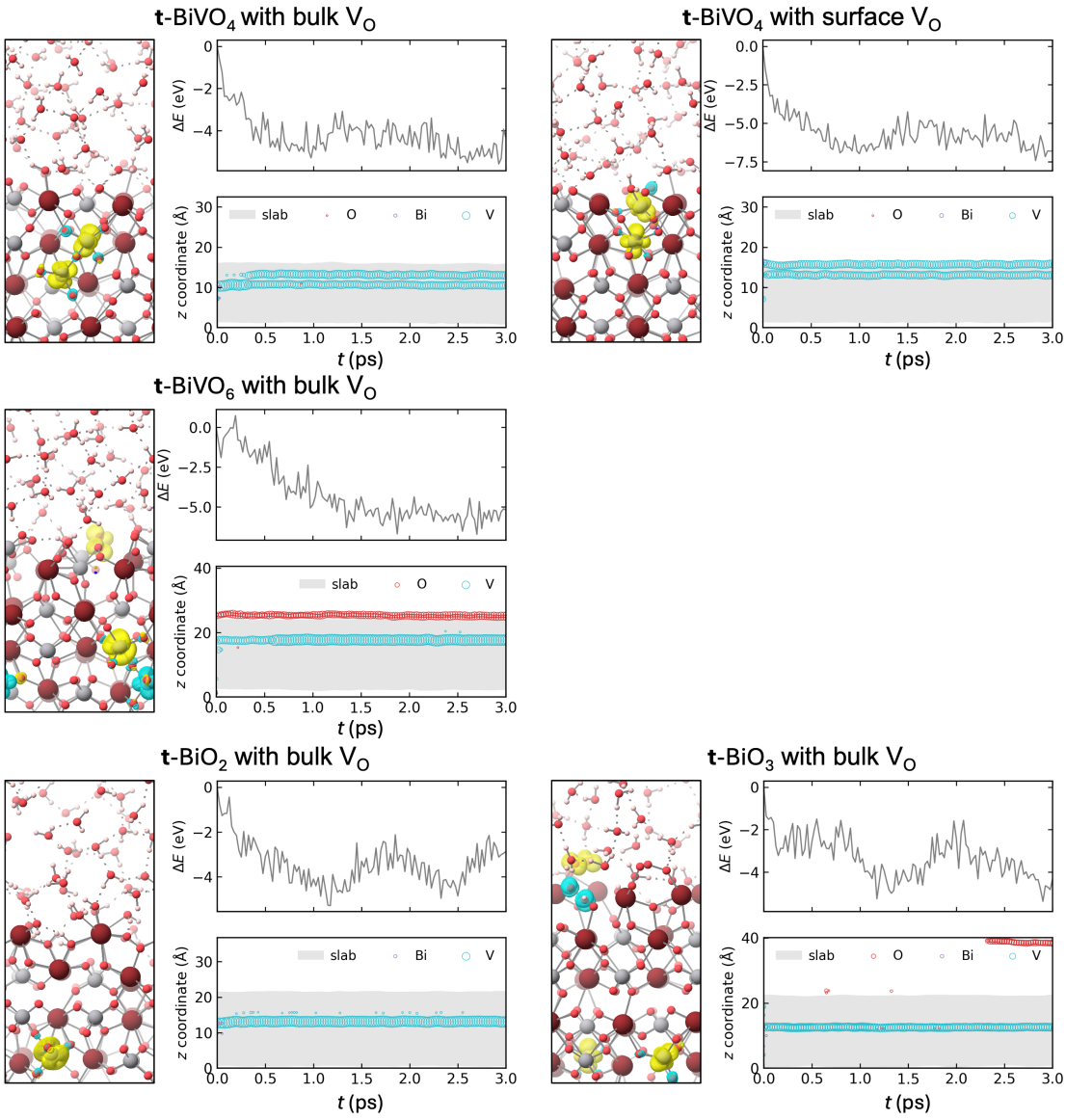

Figure S3: Representative PBE0–MD trajectories of V-centered small-polaron formation at reconstructed $BiVO_4$(010)/water interfaces. For each termination, the left panel shows a snapshot at 3 ps with spin-density isosurfaces (yellow/cyan: opposite spin channels) associated with the two excess electrons; Bi, V, and O atoms are depicted as purple, gray, and red spheres, respectively. The top-right panel plots the relaxation energy $\Delta E(t)$ upon the creation of V_O, and the bottom-right panel shows the time-resolved spin positions along the slab z-axis (the gray band marks the oxide slab; spins on O and V are colored red and turquoise, respectively).

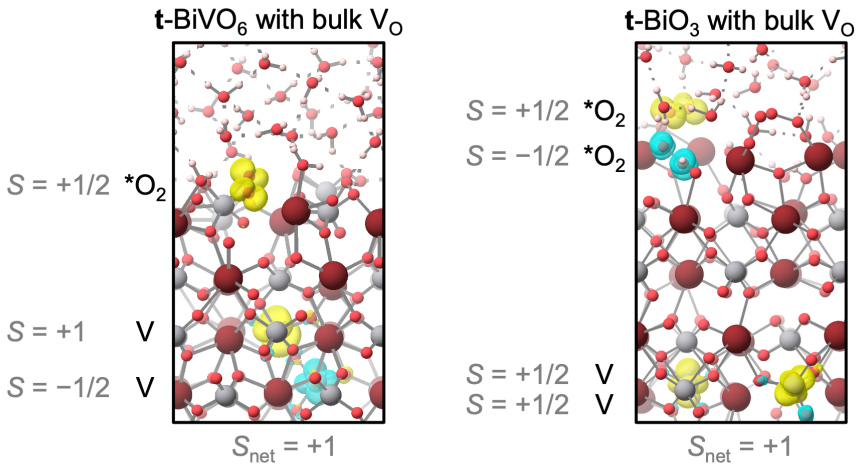

Figure S4: Spin-density isosurfaces (yellow/cyan: opposite spin channels) for reconstructed $BiVO_4(010)$/water interfaces containing a bulk-like oxygen vacancy (V_O with two injected e^-). Left: O-rich **t-**$BiVO_6$; right: Bi/O-rich **t-**BiO_3 terminations. Spins localize on a surface superoxo $*O_2^-$ (doublet) and V-centered small polarons, yielding $S_{net} = +1$ in both terminations.

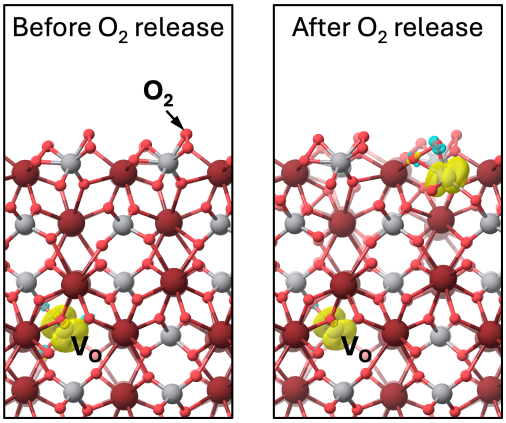

Figure S5: Spin-density isosurfaces (yellow/cyan: opposite spin channels) before and after O_2 release from **t-**$BiVO_6$ surface with a bulk-like V_O. Upon O_2 removal in the slab center, the excess electrons localize on V sites as small polarons, indicating that O_2 does not retain the excess charge under vacuum conditions.

Table S1: Bulk and surface band-edge positions (eV) for six reconstructed $BiVO_4(010)$ terminations, referenced to the vacuum level. Reported are the CBM (conduction-band minimum) and VBM (valence-band maximum); values are PBE0–MD averages over the last 2.5 ps, with standard deviations from thermal fluctuations in parentheses.

	Bulk		Surface	
Termination	VBM	CBM	VBM	CBM
t-$BiVO_4$	−6.78 (0.05)	−4.06 (0.06)	−6.66 (0.11)	−3.91 (0.13)
t-$BiVO_6$	−7.46 (0.05)	−4.74 (0.06)	−6.55 (0.20)	−4.72 (0.16)
t-BiO_2	−6.29 (0.05)	−3.57 (0.06)	−5.73 (0.19)	−3.52 (0.13)
t-BiO_3	−6.62 (0.05)	−3.90 (0.06)	−5.88 (0.21)	−4.11 (0.16)
t-VO_2	−7.80 (0.05)	−5.08 (0.06)	−7.77 (0.14)	−5.18 (0.21)
t-VO_4	−7.84 (0.05)	−5.12 (0.06)	−7.14 (0.19)	−5.13 (0.17)

References

(1) Wiktor, J.; Pasquarello, A. Electron and Hole Polarons at the $BiVO_4$–Water Interface. 2019; `https://doi.org/10.24435/materialscloud:2019.0035/v1`.

(2) Wiktor, J.; Ambrosio, F.; Pasquarello, A. Role of Polarons in Water Splitting: The Case of $BiVO_4$. *ACS Energy Lett.* **2018**, *3*, 1693–1697.

(3) Österbacka, N.; Ouhbi, H.; Ambrosio, F.; Wiktor, J. Spontaneous Oxygen Vacancy Ionization Enhances Water Oxidation on $BiVO_4$. *ACS Energy Lett.* **2023**, *9*, 153–158.

(4) Guidon, M.; Hutter, J.; VandeVondele, J. Robust Periodic Hartree-Fock Exchange for Large-Scale Simulations Using Gaussian Basis Sets. *J. Chem. Theory Comput.* **2009**, *5*, 3010–3021.

(5) Guidon, M.; Hutter, J.; VandeVondele, J. Auxiliary Density Matrix Methods for Hartree-Fock Exchange Calculations. *J. Chem. Theory Comput.* **2010**, *6*, 2348–2364.

(6) Kühne, T. D.; Iannuzzi, M.; Del Ben, M.; Rybkin, V. V.; Seewald, P.; Stein, F.; Laino, T.; Khaliullin, R. Z.; Schütt, O.; Schiffmann, F.; others CP2K: An Electronic Structure and Molecular Dynamics Software Package–Quickstep: Efficient and Accurate Electronic Structure Calculations. *J. Chem. Phys.* **2020**, *152*, 194103.

(7) Goedecker, S.; Teter, M.; Hutter, J. Separable Dual-Space Gaussian Pseudopotentials. *Phys. Rev. B* **1996**, *54*, 1703.

(8) VandeVondele, J.; Hutter, J. Gaussian Basis Sets for Accurate Calculations on Molecular Systems in Gas and Condensed Phases. *J. Chem. Phys.* **2007**, *127*, 114105.

(9) Ambrosio, F.; Wiktor, J. Strong Hole Trapping due to Oxygen Dimers in $BiVO_4$: Effect on the Water Oxidation Reaction. *J. Phys. Chem. Lett.* **2019**, *10*, 7113–7118.

(10) Wang, W.; Favaro, M.; Chen, E.; Trotochaud, L.; Bluhm, H.; Choi, K.-S.; van de Krol, R.; Starr, D. E.; Galli, G. Influence of Excess Charge on Water Adsorption on the $BiVO_4$(010) Surface. *J. Am. Chem. Soc.* **2022**, *144*, 17173–17185.

(11) Melani, G.; Wang, W.; Gygi, F.; Choi, K.-S.; Galli, G. Effects of Solvation and Temperature on the Energetics of $BiVO_4$ Surfaces with Varying Composition for Solar Water Splitting. *ACS Energy Lett.* **2024**, *9*, 5166–5171.

(12) Seo, H.; Ping, Y.; Galli, G. Role of Point Defects in Enhancing the Conductivity of $BiVO_4$. *Chem. Mater.* **2018**, *30*, 7793–7802.

(13) Wiktor, J.; Reshetnyak, I.; Ambrosio, F.; Pasquarello, A. Comprehensive Modeling of the Band Gap and Absorption Spectrum of $BiVO_4$. *Phys. Rev. Mater.* **2017**, *1*, 022401.

(14) Lee, D.; Wang, W.; Zhou, C.; Tong, X.; Liu, M.; Galli, G.; Choi, K.-S. The Impact of Surface Composition on the Interfacial Energetics and Photoelectrochemical Properties of $BiVO_4$. *Nat. Energy* **2021**, *6*, 287–294.

(15) Hilbrands, A. M.; Zhang, S.; Zhou, C.; Melani, G.; Wi, D. H.; Lee, D.; Xi, Z.; Head, A. R.; Liu, M.; Galli, G.; Choi, K.-S. Impact of Varying the Photoanode/Catalyst Interfacial Composition on Solar Water Oxidation: The Case of $BiVO_4$(010)/FeOOH Photoanodes. *J. Am. Chem. Soc.* **2023**, *145*, 23639–23650.

(16) Miceli, G.; de Gironcoli, S.; Pasquarello, A. Isobaric First-Principles Molecular Dynamics of Liquid Water with Nonlocal Van Der Waals Interactions. *J. Chem. Phys.* **2015**, *142*.

(17) Ambrosio, F.; Miceli, G.; Pasquarello, A. Structural, Dynamical, and Electronic Properties of Liquid Water: A Hybrid Functional Study. *J Phys. Chem. B* **2016**, *120*, 7456–7470.

(18) Grimme, S.; Antony, J.; Ehrlich, S.; Krieg, H. A Consistent and Accurate Ab Initio Parametrization of Density Functional Dispersion Correction (DFT-D) for the 94 Elements H-Pu. *J. Chem. Phys.* **2010**, *132*, 154104.

(19) Ambrosio, F.; Wiktor, J.; Pasquarello, A. pH-Dependent Catalytic Reaction Pathway for Water Splitting at the $BiVO_4$–Water Interface from the Band Alignment. *ACS Energy Lett.* **2018**, *3*, 829–834.

(20) Guo, Z.; Ambrosio, F.; Chen, W.; Gono, P.; Pasquarello, A. Alignment of Redox Levels at Semiconductor–Water Interfaces. *Chem. Mater.* **2018**, *30*, 94–111.

(21) Hörmann, N. G.; Guo, Z.; Ambrosio, F.; Andreussi, O.; Pasquarello, A.; Marzari, N. Absolute Band Alignment at Semiconductor–Water Interfaces Using Explicit and Implicit Descriptions for Liquid Water. *npj Comput. Mater.* **2019**, *5*, 100.

(22) Pham, T. A.; Zhang, C.; Schwegler, E.; Galli, G. Probing the Electronic Structure of Liquid Water with Many-Body Perturbation Theory. *Phys. Rev. B* **2014**, *89*, 060202.

(23) Gaiduk, A. P.; Govoni, M.; Seidel, R.; Skone, J. H.; Winter, B.; Galli, G. Photoelectron Spectra of Aqueous Solutions from First Principles. *J. Am. Chem. Soc.* **2016**, *138*, 6912–6915.

(24) Kim, T. W.; Ping, Y.; Galli, G. A.; Choi, K.-S. Simultaneous Enhancements in Photon Absorption and Charge Transport of Bismuth Vanadate Photoanodes for Solar Water Splitting. *Nat. Commun.* **2015**, *6*, 8769.